Journal of Nuclear Materials 466 (2015) 739–744

Contents lists available at ScienceDirect

Journal of Nuclear Materials

journal homepage: www.elsevier.com/locate/jnucmat

Structural stability and fission product behaviour in U_3Si

S.C. Middleburgh [a, b, *], P.A. Burr [c], D.J.M. King [a], L. Edwards [a], G.R. Lumpkin [a], R.W. Grimes [c]

[a] IME, Australian Nuclear Science and Technology Organisation, Lucas Heights, New South Wales, Australia
[b] Westinghouse Electric Sweden AB, SE-72163 Västerås, Sweden
[c] Department of Materials, Imperial College London, South Kensington, London SW7 2AZ, United Kingdom

ARTICLE INFO

Article history:
Received 28 January 2015
Received in revised form
17 March 2015
Accepted 28 April 2015
Available online 7 May 2015

ABSTRACT

The crystalline and amorphous structures of U_3Si have been investigated using density functional theory techniques for the first time. The effects of disorder and the impact of fission products has been separated to understand the swelling characteristics of U_3Si in both crystalline and amorphous U_3Si. Initially, the stability of the three experimentally observed polymorphs of U_3Si were explored. Subsequently, we modelled the amorphous U_3Si system and conclude that initial increase in volume observed experimentally at low temperature corresponds well with the volume change that occurs with the observed amorphisation of the material. The solubility of Xe and Zr into both the crystalline and amorphous systems was subsequently investigated.

1. Introduction

There is growing interest in the use of alternative fuels in light water reactors. The impetus can be considered from two perspectives: economic and safety. Economically, the higher density fuels exhibit improved uranium loading allowing manufacturers to sell the assemblies at a premium. More importantly, the safety characteristics of such fuels can be improved markedly over conventional UO_2 pellets held within a Zr-alloy cladding (materials can be chosen with better oxidation resistance [1] or lower susceptibility for degradation due to hydrogen pick-up [2–4], for example), and the enrichment of the fuel can be reduced owing to the greater ^{235}U density.

Uranium silicides show a great deal of promise as next generation nuclear fuels. The densities of U_3Si and U_3Si_2 are 15.4 g/cm^3 and 12.2 g/cm^3, respectively, with maximum uranium loadings of 14.6 g/cm^3 and 11.3 g/cm^3, respectively [5]. In comparison, uranium dioxide has a density of 10.96 g/cm^3 [6] with a maximum uranium loading of 9.66 g/cm^3. Additionally, as the compounds exhibit metallic bonding, the thermal conductivities are significantly higher than UO_2 [7], especially after irradiation [8,9]. The UO_2 system degrades significantly because the defect population shortens the mean free path of phonons, which are the main transmitter of heat in ionic solids. Conversely, intermetallic compounds are much less affected by irradiation since of the heat transmission process is mainly electronic.

U_3Si becomes amorphous at low temperatures and moderately low damage (~0.3 displacements per atom up to ~500 K, see Fig. 1) [10–12]. As the fuel has been used mainly as a dispersant in Al plate fuel in research reactors, this swelling has not been a significant limiting factor, especially at low temperatures, although it is a property that has attracted a great deal of attention [13–16]. The drive to manufacture pellets of silicide fuel for use in light water reactors means that a deeper understanding of swelling is required. Here we investigate the structure of crystalline U_3Si and present a method to model amorphous U_3Si.

Past experimental studies, such as work by Hastings and Stoute [15], have highlighted the temperature and burnup dependence of the swelling behaviour of U_3Si. Fig. 1 shows the observed trend in volume change of U_3Si taken from four different fuel elements (see [15] for details). The observed onset of swelling corresponds to the temperature range over which U_3Si is expected to remain crystalline regardless of the dose (measured in displacements per atom, dpa). This is highlighted by the swelling occurring at higher temperatures than the two reported curves for critical amorphisation dose (one as-sintered sample and one heat treated sample –

* Corresponding author at: IME, Australian Nuclear Science and Technology Organisation, Lucas Heights, New South Wales, Australia.
E-mail address: simon.middleburgh@hotmail.co.uk (S.C. Middleburgh).

http://dx.doi.org/10.1016/j.jnucmat.2015.04.052
0022-3115/

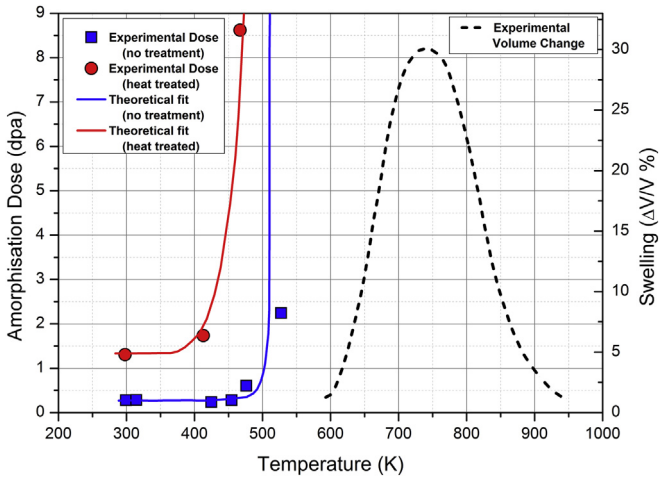

Fig. 1. Calculated (lines) and measured (data points) temperature dependence of amorphisation dose with 1.5 MeV Kr ions in U_3Si, with (red) and without (blue) pre-treatment [7]. The dashed line reports the experimentally obtained volume change as a function of calculated irradiation dose for a series of fuel elements [15]. (For interpretation of the references to colour in this figure legend, the reader is referred to the web version of this article.)

adapted from Rest 1997 [10]). The swelling, seen to be quite severe at the intermediate temperatures of 750 K, is thought to be due to the homogeneous nucleation and growth of voids (similar to those observed in uranium metal [17] and other metallic systems). The mobility and growth of these voids would be rapid at temperatures above the critical temperature for amorphisation as this temperature also suggests that the defect population is highly mobile (preventing point defect build up and loss of crystal structure). The reduced swelling at lower temperatures corresponds to the situation where the material is expected to be amorphous. This variation in swelling is highlighted in Fig. 2, which shows the change in volume of two samples irradiated at two temperatures: one below the critical temperature for amorphisation and the other above.The absence of run-away swelling in the cooler, amorphous sample, may be a result of the difference in defect and fission product accommodation/mobility in the structure as one may expect the coalescence and nucleation of these defects to differ from the crystalline, high temperature system (a change in swelling rate may occur at higher exposures). This change in thermodynamic drive for defect nucleation may retard or halt the void growth and will be explored on the atomic scale in this work.

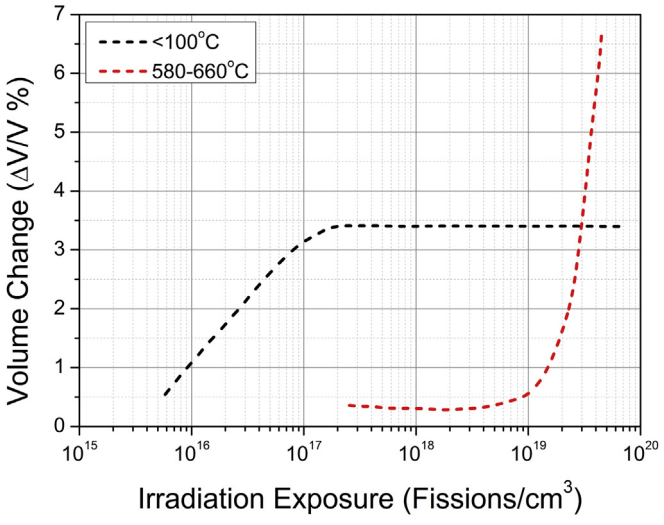

Fig. 2. Experimental volume increase as a function of irradiation exposure for U_3Si at two centre line fuel temperatures (adapted from [10]).

Understanding the behaviour of fission products in nuclear fuel is of paramount importance to ensure their safe operation and optimum performance. A huge amount of work has been carried out to understand the behaviour of fission products in UO_2, both experimentally [18,19] and theoretically [20–22]. To qualify new fuels for use in commercial reactors, equivalent data is required for the development of a safety case. Here we contribute to this effort by simulating the behaviour of two chemically very different fission products Xe and Zr.

2. Methodology

Atomic scale calculations were carried out using density functional theory (DFT) to describe the inter-atomic bonding. Since U_3Si exhibits metallic bonding, DFT is a suitable simulation method [23,24].

The calculations employed the GGA exchange correlation function with spin-polarisation effects also included. Temperature dependent thermodynamics properties were calculated within the harmonic approximation by performing phonon density of state simulations using the CASTEP code [25]. The structures were optimised to Hellmann–Feynman forces on atoms less than 10^{-} eV/nm. Phonon properties were evaluated using the direct method with supercell extrapolation [26,27]. Supercells of up to 216 atoms were employed. Variations in thermodynamical properties (enthalpy, heat capacity and Helmholtz free energy) between supercells containing 64 and 216 atoms were less then 1% of their absolute value.

The Vienna Ab-initio Simulation Package (VASP [28,29]) was used to investigate the amorphous U_3Si system and behaviour of Xe and Zr, two fission products, in crystalline and amorphous U_3Si. The pseudopotentials supplied in the VASP package, which use the projector augmented wave formalism, were used to investigate the amorphous structure. Each supercell was fully geometry optimised under constant pressure with a convergence stopping energy of 10^{-3} eV per supercell (similar to calculations carried out previously [23,24,30]). A Methfessel–Paxton smearing method was used for all calculations with a tailored value of 0.125 eV.

Defect calculations were carried out on a β-U_3Si supercell (the room temperature structure) containing 108 lattice sites (81 uranium sites and 27 silicon sites).

Amorphous U_3Si was investigated using a similar method to a recent article that investigated the V–Zr amorphous system [30]. 15 unique and randomly populated supercells (containing 108 atoms) were created and relaxed under constant pressure. The properties of the amorphous systems were simulated by randomly assigning U and Si to x, y, z coordinates with a restriction of no atoms placed within 0.15 nm of each other. As highlighted in the previous work: the systems were relaxed from a significantly lower density (5%) to the expected final density to prevent imaging/density effects ordering the system. The average radial distribution functions of the system were obtained for each of the systems using the Forcite program.

The effect of the common fission products Xe and Zr on the swelling of the system were subsequently investigated. Xe solution was considered from its elemental gas, while Zr solution was considered from Zr_3Si [31]. Zr_3Si was used as the reference product as it maintains the U:Si stoichiometry.

3. Results

3.1. The U_3Si crystal structure

The U_3Si structure is similar to the reported U_3Si_2 structure [32].

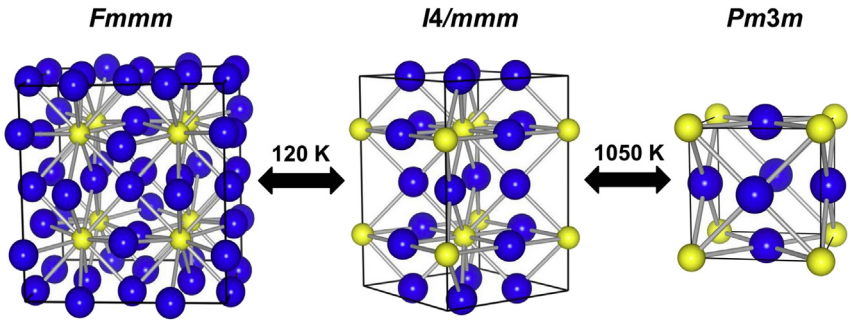

Fig. 3. The three reported crystalline structures of U_3Si and their transition temperatures (as reported by [32]).

It forms three different crystal structures [32]: a *Fmmm* below 120 K (termed α-phase) which transforms to a higher symmetry *I4/mmm* at 120 K (termed β-phase) which in turn is reported to transform to a high symmetry *Pm3m* structure at temperatures above 1050 K (termed γ-phase). All structures are highly related and are illustrated in Fig. 3.

Phonon density of states were calculated for the three polymorphs of U_3Si. From these, the Helmholtz free energy change with temperature was derived using the harmonic approximation, see Fig. 4. The low-symmetry α-U_3Si remains the most stable phase until ~250 K (i.e. it has the most negative free energy), at which point β-U_3Si becomes more favourable. The β structure exhibits a free energy curve that only slightly steeper than that of the α structure. Consequently, there is a large temperature range (~100 K) around the $\alpha \rightarrow \beta$ transition in which the difference in energy between the two polymorphs is within the accuracy of the methodology. As a result, we cannot accurately predict the transition temperature and is somewhat higher than the reported value [33].

At higher temperature a displacive transformation from β-U_3Si to γ-U_3Si is expected from experimental data. Conversely, our simulations show that the γ phase is unstable at all temperatures. Crystallographically, the difference between the two structures is very small: β-U_3Si can be thought of a lower symmetry form of γ-U_3Si, in which a plane containing U atoms (any of the three planes) has been rotated with respect to its normal. Due to the cubic symmetry of γ-U_3Si, there are 6 equivalent ways in which such transformation may occur. In β-U_3Si, rotation of the planes causes atomic displacements of 0.0145 nm for the U atoms involved. At high temperatures, displacements are readily obtained due to thermal vibrations. Therefore, it is reasonable that at high temperature, β-U_3Si may exhibit local fluctuations in the ordering of these displacements. In turn, these fluctuations should cause an effective averaging of the U positions, when observed globally (i.e. using electron or X-ray diffraction techniques which probes a volume of material), which is observed as a high symmetry cubic structure. An analogous phenomenon has been reported in perovskite oxide material $BaZrO_3$ [34]. The order/disorder transition is highlighted by the experimental observations of twinning in the U_3Si system [12,35,36].

3.2. Amorphous U_3Si

U_3Si is observed to amorphise at low temperatures and a moderate-to-low damage dose. Here we attempt to simulate the structure of the amorphous material and compare it to the perfect tetrahedral U_3Si structure that forms at room temperature. An example of one of the relaxed supercells is shown in Fig. 5. All supercells were initially cubic but after relaxation at constant pressure, the cells distorted to triclinic symmetry.

Compared to the room temperature, β-U_3Si system, the amorphous supercells, on average, swelled 3.66% in volume (with a standard deviation of 0.39%). This value compares extremely well with the experimental swelling observed in U_3Si at low temperature by Hastings and Stoute [15], illustrated in Fig. 3, even though

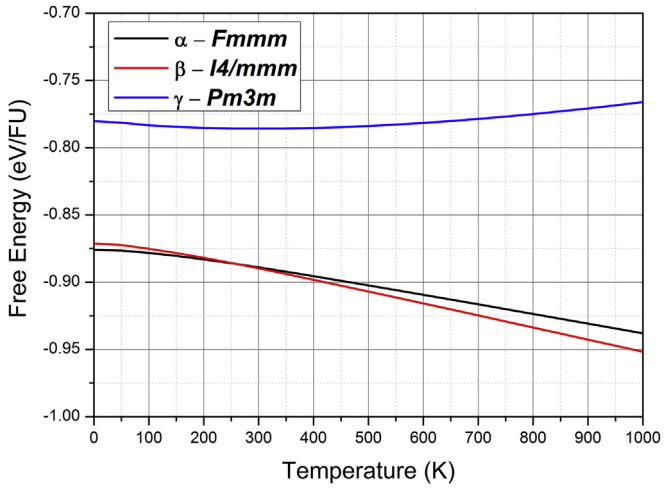

Fig. 4. Variation in formation energy of α-U_3Si (black), β-U_3Si (red) and γ-U_3Si (blue) with temperature. (For interpretation of the references to colour in this figure legend, the reader is referred to the web version of this article.)

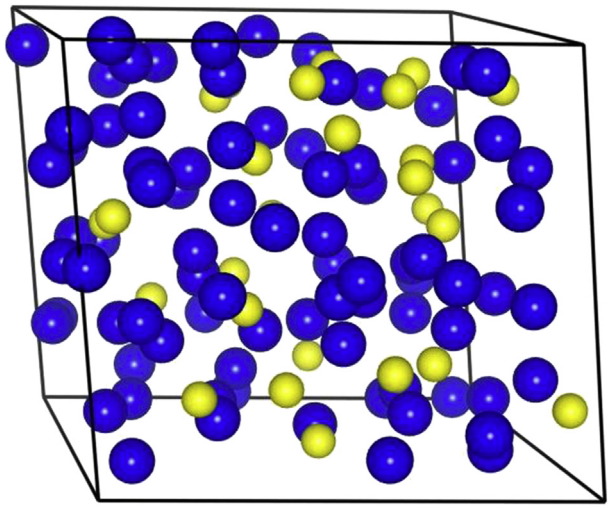

Fig. 5. Example of supercell used to simulate the amorphous structure of U_3Si.

the static nature of the calculations presented here cannot take account of thermal effects.

The simulated radial distribution function for the amorphous U_3Si, produced by averaging the individual radial distribution functions for each relaxed supercell, is reported in Fig. 6. The pattern highlights some significant short range order that diminishes at intermediate separations. The two shorter bond lengths highlighted by the RDF plot are centred at 0.259 nm and 0.287 nm. These bonds correspond to the shortest U–U bond and U–Si bond, respectively, similar to the crystalline bond lengths in all three reported U_3Si structures. The RDF is consistent with metallic and metalloid amorphous alloys including that of Pd_4Si [37].

An X-ray diffraction pattern has been simulated for amorphous U_3Si in Fig. 7 and is plotted with experimental data taken from U_3Si that has been subject to both Ar implantation [38] and neutron exposure [39]. The maximum intensity of these two peaks are located at identical 2θ positions. Smaller peaks are observed with lower intensities in both experimental patterns which suggests these structures are not fully amorphous. The Ar damaged sample's main peak is shifted towards the higher 2θ values corresponding to slightly smaller bond lengths (possibly due to the interaction of the Ar with the amorphous material or a deviation in stoichiometry of the material from ideal U_3Si). Other data reported by Walker [38], suggests that samples irradiated to higher fluences of ~10^{17} ions/cm^2 do not show any extra peaks other than the main diffuse peak that is predicted in our work. The amorphous structural model presented in this work is therefore consistent with experimental data. On this basis it will be used as the basis for modelling.

The solubility of the two fission products Xe and Zr in amorphous U_3Si is now investigated. These results will be compared to values calculated for crystalline U_3Si.

3.3. Accommodation of Xe and Zr in the U_3Si lattice

3.3.1. Accommodation in amorphous U_3Si

Both Xe and Zr were introduced into the amorphous U_3Si supercells to understand the influence of these fission products on swelling and to derive a measure of their approximate solution/segregation enthalpies from their respective states (Xe from its mono-atomic gas and Zr from the silicide Zr_3Si [31]). We chose Zr_3Si for simplicity as it will not change the overall stoichiometry of the system.

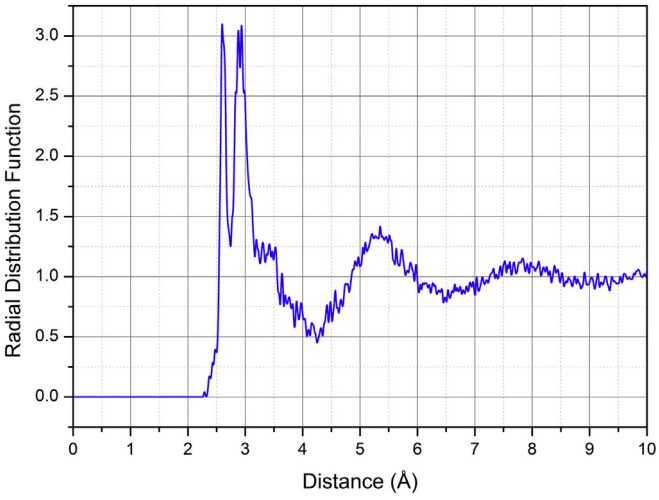

Fig. 6. The radial distribution function (RDF) of the amorphous U_3Si structure, constructed by averaging the RDF values of all supercells that were calculated using the Forcite program.

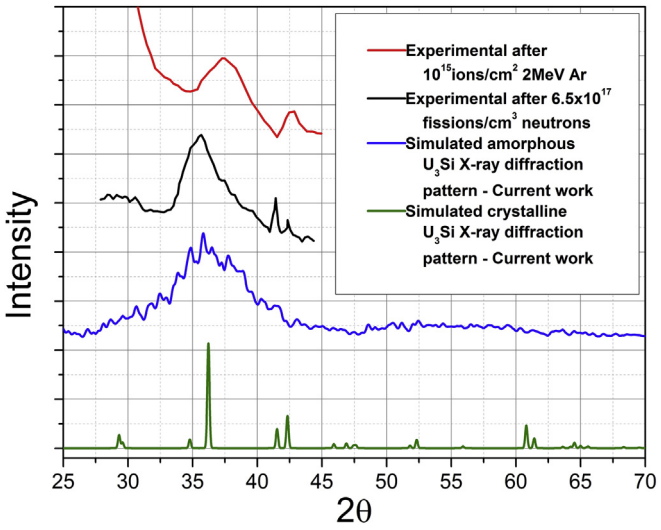

Fig. 7. Experimental X-ray diffraction patterns compared to a simulated amorphous U_3Si pattern (obtained using a method developed previously [30]) and a simulated crystalline U_3Si pattern. The line is data obtained by 2 MeV Ar irradiation of U_3Si to 1015 ions/cm^2 [39]. The black line is data obtained by neutron irradiation of U_3Si with a fission density of 6.5×10^{17} [39]. The blue line is the simulated amorphous diffraction pattern from this work. The green line is the simulated crystalline diffraction pattern from this work. (For interpretation of the references to colour in this figure legend, the reader is referred to the web version of this article.)

When Xe is added to the supercell a small swelling is observed when compared to the un-doped amorphous system (1.9% larger volume). The concentration of Xe in the supercell is 0.92 at.% (approximately an order of magnitude greater than can be expected in a UO_2 LWR pellet). Compared to the swelling associated with the material becoming amorphous, the swelling that occurs as a result of the Xe being held 'in solution' within the amorphous material is small. The solution enthalpy of Xe compared to its mono-atomic gas was calculated to be 4.19 eV: unfavourable but lower than the calculated solution enthalpies for Xe in UO_2. Further, the lack of a fast diffusion pathway will also limit the release of Xe from the lattice and the formation and growth of large bubbles within the lattice and at grain boundaries.

An additional Xe atom was subsequently placed within the lattice to understand the drive for Xe nucleation in the amorphous material. The solution enthalpy was 0.15 eV less favourable per Xe compared to the isolated Xe atom in U_3Si solution. As such there is no drive for nucleation of Xe in the amorphous material.

The influence of Zr, the most abundant fission product in ^{235}U containing fuel, was also investigated. Zr_3Si has been observed experimentally and it is this compound that the solubility of Zr in amorphous U_3Si is compared with. Firstly, the volume increase when Zr is incorporated into U_3Si (substituting for a U atom) is low (0.34%). The solution energy for Zr_3Si to enter amorphous U_3Si was calculated to be 0.78 eV. This is a moderate energy, consistent with a small concentration of Zr held within the amorphous U_3Si structure with a small entropic contributions (similar to the partially soluble fission products such as La in UO_2 [22]) and the remainder forming a Zr containing precipitate (Zr_3Si being the likely binary compound).

3.3.2. Incorporation of Xe and Zr in crystalline U_3Si

The solution of a Xe atom onto an interstitial position demands an energy of 9.41 eV via the following reaction:

$$Xe(g) \rightarrow Xe_i \quad (1)$$

Accommodation of Xe on to pre-existing U and Si vacancies proceeds with energies of 6.45 eV and 3.40 eV, respectively. Solution energies, forming mono-atomic U or Si, are 7.48 eV and 7.13 eV. Xe is as such predicted to be highly insoluble in crystalline U_3Si and therefore there is a strong drive for bubble formation.

Accommodation of Zr metal onto pre-existing U and Si vacancies is calculated to proceed with energies of −1.53 eV and −1.79 eV. It is surprising that the energy for the accommodation of Zr onto the Si site is more favourable than for the U site given the similarity between Zr and U metal. Solution, producing mono-atomic U and Si is predicted to proceed with energies of −0.51 eV and 1.95 eV. Solution of Zr onto an interstitial site exhibits an energy of 3.00 eV: relatively unfavourable compared to the substitutional defects.

Zr_3Si is also calculated to be stable (and has been observed). It forms from Si and Zr via the following reaction 2 releasing 5.16 eV of energy:

$$3Zr + Si \rightarrow Zr_3Si \quad (2)$$

Zr in the form of Zr_3Si is predicted to go into solution within U_3Si via the following reaction:

$$Zr_3Si + 3U_U \rightarrow 3Zr_U + U_3Si \quad (3)$$

This has an energy of −3.70 eV, meaning that Zr is predicted to be highly soluble in U_3Si regardless of the form that it takes. This is different to UO_2 fuel behaviour as Zr readily segregates to form ZrO_2 and perovskite zirconates [18,40].

4. Summary

Atomic scale simulations have been carried out that help understand the stability of the U_3Si system. The α to β phase transformation was predicted to occur at a slightly higher than expected temperature of 250 ± 50 K (compared to the experimentally observed value of 120 K). This small discrepancy may be a result of approximations in the computational technique. It may also be however that the energy barrier for transformation is large enough to prevent the transformation until lower temperatures.

The high symmetry, cubic γ-U_3Si structure was not predicted to become stable with respect to the α and β phases at any temperature. We have discussed the possible reasons for this and suggest that locally the bonding remains tetragonal (or similar) but thermal fluctuations at this high temperature 'average' the bulk structure to produce the high symmetry observations. This hypothesis has been suggested previously to explain the discrepancies between the X-ray diffraction and transmission electron microscopy results with Raman spectroscopy data for $BaZrO_3$ [34].

The experimental volume change associated with the crystalline to amorphous transition induced by neutron radiation has been well reproduced by the simulations in this work. Our method has been shown to be versatile and useful in past work and removes the need for costly melt/quench cycles, however, care must be taken in highly covalent/ionic systems. The RDF shows some short range order as expected in an amorphous solid.

The simulated X-ray diffraction pattern for the amorphous U_3Si system agrees remarkably well with experimental observations. The satellite peaks associated with the experimental techniques are not entirely reproduced by the simulation although it should be noted that experiments which expose U_3Si to higher radiation doses provide patterns without these peaks [39].

Xe is predicted to be far more soluble in amorphous U_3Si compared to the crystalline material. This has significant implications for the behaviour of the fuel. Clustering is also predicted to be unfavourable for Xe in the amorphous U_3Si (potentially limiting the bubble/void growth and run-away swelling). An increase in temperature may allow the re-crystallisation of the silicide to take place, markedly changing the solubility of the Xe, which will be able to diffuse via a lower energy pathway and form gas bubbles rapidly. This behaviour alone may mean maintaining the fuel at a temperature above the critical temperature for amorphisation. However, as we have already discussed, past work shows that the crystalline material is susceptible to run-away swelling induced by damage and fission products and dopants may be designed to be added to U_3Si to maintain the amorphous structure to higher temperatures.

Zr, on the other hand, is predicted to be stable into crystalline U_3Si but only partially soluble in the amorphous material (when forming crystalline Zr_3Si). The precipitation of Zr-rich precipitates in amorphous U_3Si may act as a sort of nucleation site (although defect diffusion will be limited as a result of the amorphous structure), however one may expect this silicide to amorphise in a similar manner to U_3Si, certainly a phenomenon that warrants further work.

Indeed, there is a much further work required to better understand U_3Si system as well as the other members of the uranium–silicon system, for example U_3Si_2. The prediction for stability of other fission products and the effect of stoichiometry will be important in order that the viability of this system as a nuclear fuel for commercial power reactors can be assessed. Experimental verification of these results and other material properties is integral to the successful implementation of these materials in the next generation of commercial light water reactor fuels.

Acknowledgements

This work was carried out as part of the Consortium for Advanced fuels for enhanced Accident Tolerance (CARAT) collaboration. In this regard, we would like to thank Lars Hallstadius, Peng Xu and Edward Lahoda for useful discussions. This research was undertaken with the assistance of resources provided at the NCI National Facility systems at the Australian National University through the National Computational Merit Allocation Scheme supported by the Australian Government. This work was supported by the Multi-modal Australian ScienceS Imaging and Visualisation Environment (MASSIVE) (www.massive.org.au).

References

[1] J.T. White, A.T. Nelson, D.D. Byler, D.J. Safarik, J.T. Dunwoody, K.J. McClellan, J. Nucl. Mater. 456 (2014) 442–448.
[2] S.C. Lumley, R.W. Grimes, S.T. Murphy, P.A. Burr, A. Chroneos, P.R. Chard-Tuckey, M.R. Wenman, Acta Mater. 72 (2014) 351–362.
[3] H. Wang, A. Chroneos, C. Jiang, U. Schwingenschlögl, Phys. Chem. Chem. Phys. 15 (2013) 7599–7603.
[4] J. Zheng, X. Zhou, L. Mao, H. Zhang, J. Liang, L. Sheng, S. Peng, Int. J. Hydrogen Energy (2015), http://dx.doi.org/10.1016/j.ijhydene.2015.02.045 (in press).
[5] R.F. Domagala, T.C. Wiencek, H.R. Thresh, Nucl. Technol. (1983).
[6] J.K. Fink, J. Nucl. Mater. 279 (2000) 1–18.
[7] J. Hastings, J.R. MacEwan, L.R. Bourque, J. Am. Ceram. Soc. 55 (1972) 240–242.
[8] M.J. Qin, M.W.D. Cooper, E.Y. Kuo, M.J.D. Rushton, R.W. Grimes, G.R. Lumpkin, S.C. Middleburgh, J. Phys.: Condens. Matter 26 (2014) 495401.
[9] Q. Yin, S.Y. Savrasov, Phys. Rev. Lett. 100 (2011) 225504.
[10] J. Rest, J. Nucl. Mater. 240 (1997) 205–214.
[11] R.C. Birtcher, L.M. Wang, Nucl. Instrum. Meth. B 59/60 (1991) 966–969.
[12] B. Bethune, J. Nucl. Mater. 40 (1971) 205–212.
[13] J.L. Snelgrove, G.L. Hofman, M.K. Meyer, C.L. Trybus, T.C. Wiencek, Nucl. Eng. Des. 178 (1997) 119–126.
[14] J. Rest, G.L. Hofman, J. Nucl. Mater. 210 (1994) 187–202.
[15] I.J. Hastings, R.L. Stoute, J. Nucl. Mater. 37 (1970) 295–302.
[16] I.J. Hastings, J. Nucl. Mater. 41 (1971) 195–202.
[17] S.F. Pugh, J. Nucl. Mater. 4 (1961) 177–199.
[18] H. Kleykamp, J. Nucl. Mater. 131 (1985) 221–246.
[19] J.A. Turnbull, C.A. Friskney, J. Nucl. Mater. 58 (1975) 31–38.
[20] R.W. Grimes, C.R.A. Catlow, Philos. Trans. R. Soc. S.-A. 335 (1991) 533.
[21] M.L. Fullarton, M.J. Qin, M. Robinson, N.A. Marks, D.J.M. King, E.Y. Kuo, G.R. Lumpkin, S.C. Middleburgh, J. Mat. Chem. A 1 (2013) 14633–14640.

[22] S.C. Middleburgh, D.C. Parfitt, R.W. Grimes, B. Dorado, M. Bertolus, P.R. Blair, L. Hallstadius, K. Backman, J. Nucl. Mater. 420 (2012) 258–261.
[23] M.L. Fullarton, R.E. Voskoboinikov, S.C. Middleburgh, J. Alloy Comp. 587 (2014) 794–799.
[24] J. Yanga, J. Longb, L. Yangb, D. Li, J. Nucl. Mater. 443 (2013) 195–199.
[25] S.J. Clark, M.D. Segall, C.J. Pickard, P.J. Hasnip, M.I.J. Probert, K. Refson, M.C. Payne, Zeitschrift Für Kristallographie 220 (2005) 567–570.
[26] W. Frank, C. Elsässer, M. Fähnle, Phys. Rev. Lett. 39 (1995) 346.
[27] K. Parlinski, Z.Q. Li, Y. Kawazoe, Phys. Rev. Lett. 78 (1997) 4063–4066.
[28] G. Kresse, J. Hafner, Phys. Rev. B 47 (1993) 558.
[29] G. Kresse, J. Hafner, Phys. Rev. B 49 (1994) 4251.
[30] D.J.M. King, S.C. Middleburgh, A.C.Y. Liu, H.A. Tahini, G.R. Lumpkin, M.B. Cortie, Acta Mater. 83 (2015) 269–275.
[31] H. Okamoto, Bull. Alloy Phase Diagrams 11 (1990) 513.
[32] K. Remschnig, T. Le Bihan, H. Noël, P. Rogl, J. Solid State Chem. 97 (1992) 391.
[33] G. Kimmel, B. Sharon, M. Rosen, Acta Cryst. B36 (1980) 2386–2389.
[34] S.C. Middleburgh, I. Karatchevtseva, B.J. Kennedy, P.A. Burr, Z. Zhang, E. Reynolds, R.W. Grimes, G.R. Lumpkin, J. Mat. Chem. A 2 (2014) 15883–15888.
[35] G. Kimmel, J. Nucl. Mater. 89 (1980) 402–404.
[36] J.F.R. Ambler, J. Nucl. Mater. 22 (1967) 112–114.
[37] P.H. Gaskell, J. Non-Cryst. Solids 32 (1979) 207–224.
[38] D.G. Walker, J. Nucl. Mater. 37 (1970) 48–58.
[39] B. Bethune, J. Nucl. Mater. 31 (1969) 97–202.
[40] M.W.D. Cooper, S.C. Middleburgh, R.W. Grimes, J. Nucl. Mater. 438 (2013) 238–245.